Journal: *Hydrology and Earth System Sciences*

Manuscript type: Research Article

Impacts of high inter-annual variability of rainfall on a century of extreme hydrological regime of northwest Australia

A. Rouillard[1], G. Skrzypek[1], S. Dogramaci[1,2], C. Turney[3], and P. F. Grierson[1]

[1]West Australian Biogeochemistry Centre and Ecosystems Research Group, School of Plant Biology, The University of Western Australia, Crawley, WA 6009, Australia

[2]Rio Tinto Iron Ore, Perth, WA 6000, Australia

[3]Climate Change Research Centre, University of NSW, Sydney, NSW 2052, Australia

Correspondence to: A. Rouillard (alexandra.rouillard@research.uwa.edu.au, alexandrarouillard@yahoo.ca)

Abstract

Long-term hydrological records provide crucial reference baselines of natural variability that can be used to evaluate potential changes in hydrological regimes and their impacts. However, there is a dearth of studies of the hydrological regimes for tropical drylands where intraseasonal and interannual variability in magnitude and frequency of precipitation are extreme. Here, we sought to identify the main hydroclimatic determinants of the strongly episodic flood regime of a large catchment in the semi-arid, subtropical northwest of Australia and to establish the background of hydrologic variability for the region over the last century. We used a monthly sequence of satellite images to quantify surface water expression on the Fortescue Marsh, the largest water feature of inland northwest Australia, from 1988 to 2012. We used this sequence together with instrumental rainfall data to build a statistical model with multiple linear regression and reconstruct monthly history of floods and droughts since 1912. We found that severe and intense regional rainfall events, as well as the sequence of recharge events both within and between years, determine surface water expression on the floodplain (i.e., total rainfall, number of rain days and carried-over inundated area; $R^2_{adj} = 0.79$; p value < 0.001, $E_{RMSP} = 56$ km^2). The most severe reconstructed inundation over the last century was in March 2000 (1000 km^2), which is less than the 1300 km^2 area required to overflow to the adjacent catchment. The Fortescue Marsh was completely dry for 32% of all years, for periods of up to four consecutive years. Extremely wet years (seven of the 100 years) caused the Marsh to remain inundated for up to 12 months; only 25% of years (9% of all months) had floods of greater than 300 km^2. The prolonged, severe and consecutive yearly inundations between 1999 and 2006 were unprecedented compared to the last century. While there is high inter-annual variability in the system, if the frequency and intensity of extreme rainfall events for the region were to increase (or be similar to 1999–2006), surface water on the Marsh will become more persistent, in turn impacting its structure and functioning as a wetland.

1 Introduction

Quantifying the hydrological response to changes in rainfall patterns remains challenging in arid environments, especially for remote tropical and minimally-gauged drylands such as the Pilbara region of northwest Australia. Tropical drylands are often characterised by extreme hydroclimatic conditions, where rainfall is highly heterogeneous in its distribution and the majority of streams and rivers are ephemeral but highly responsive to intense rainfall events. For example, peak surface flow rates generated from ephemeral rivers and creeks in the Pilbara can reach thousands of cubic metres per second after such events (WA Department of Water, 2014). These factors contribute to high spatial and temporal heterogeneity of recharge-discharge mechanisms across any one catchment, which in turn presents considerable challenges for predicting of resultant impacts of hydroclimate change on catchment hydrology. Several lines of evidence suggest the Pilbara has been particularly wet during the late 20th century (e.g., Cullen and Grierson, 2007; Shi et al., 2008; Taschetto and England, 2009; Fierro and Leslie, 2013) and that the frequency of extreme precipitation events may be increasing (e.g., Gallant and Karoly, 2010). However, there is no consensus on whether the observed higher summer rainfall can be attributed to an overall 'wettening trend' or whether the recent 'wet' period may be a feature within the range of natural 'extreme' variability characteristic of this region. The consequences of intensification and shifts in frequency of the hydrological cycle as well as greater variability of precipitation patterns have already been documented in other parts of the world, including alterations in the seasonality and extent of floods or drought (Harms et al., 2010; Feng et al., 2013).

Ecological disturbances such as flood and drought cycles are usually described by their extent, spatial distribution, frequency (or return interval), predictability and magnitude (i.e., severity, intensity and duration) (White and Pickett, 1985). Determining how altered hydrologic regimes (floods and droughts) may in turn impact vulnerable ecosystems, including wetlands, requires detailed understanding of the links between the distribution of precipitation and flows across multiple spatial and temporal scales (e.g., Kiem et al., 2003; Kiem et al., 2004; Verdon-Kidd and Kiem, 2009; Ishak et al., 2013). The Pilbara region of northwest Australia, in common with other hot arid regions of the world including the Indian Thar, Namib-Kalahari and Somali deserts, is characterised by some of the most variable annual and inter-annual rainfall patterns on the planet (van Etten, 2009). In the Pilbara,

tropical cyclones and other low-pressure systems forming off the west Australian coast in the tropical Indian Ocean often result in severe flooding events (WA Department of Water, 2014). These events punctuate years of prolonged drought, which together define the "boom-bust" nature of productivity in highly variable desert ecosystems (McGrath et al., 2012). Surface water availability or persistence of water features, physical disturbances and hydrological connectivity resulting from this highly dynamic regime in turn play a central role in shaping aquatic and terrestrial ecosystem processes, species life history strategies and interactions and population dynamics (Box et al., 2008; Leigh et al., 2010; Pinder et al., 2010; Sponseller et al., 2013). Changes in hydroclimatic patterns and extremes that might alter the natural disturbance regime would thus have profound consequences for the structure and functioning of often highly specialised and adapted arid ecosystems (Newman, 2006; Leigh et al., 2010).

Remote sensing has proven to be the most suitable and often only tool for investigating spatial and temporal variability of ~~arid zone remote~~ wetlands in the arid zone (e.g., McCarthy et al., 2003; Bai et al., 2011; Thomas et al., 2011) and improved understanding of ecohydrological processes at the regional scale particularly (Gardelle et al., 2010; Haas et al., 2011; McGrath et al., 2012). High temporal resolution is also needed to accurately characterise the seasonal cycles and mechanisms that generate the complex spatial and temporal patterning of floods at basin and regional scales and to effectively address the consequences of changes in disturbance regimes for different ecosystems. For example, satellite imagery has recently been successfully combined with hydrological modelling to extend wetland flood regime records from tropical Australia (e.g., Karim et al., 2012) and to investigate mechanisms such as connectivity among floodplains (e.g., Trigg et al., 2013). Similar approaches have also been used to understand the evolution of daily flood and dynamics of floodplain vegetation on the east coast of Australia (Powell et al., 2008). Remote sensing techniques have also been utilised to calibrate hydraulic models of dynamic flow processes during floods, albeit over relatively short time periods (e.g., Bates, 2012; Neal et al., 2012; Wen et al., 2013). However, flood regime analyses based solely on remotely-sensed data do not adequately capture the lengthy temporal scales of flood and drought cycles in many arid and semi-arid regions, which require calibration periods that encompass variability at interannual, decadal and multidecadal scales, especially to elucidate relationships with climatic drivers and geomorphological processes (Roshier et

al., 2001; Mori, 2011; Ishak et al., 2013; Kiem and Verdon-Kidd, 2013).

Here, we sought to identify the main hydroclimatic determinants of flooding regimes at the catchment scale and to establish the background of variability of surface water expression over the last century in the semi-arid northwest of Australia. First, we identified the main rainfall variables that influence surface water expression on the Fortescue Marsh, the largest internally draining wetland in the Pilbara region (Fig. 1), by combining monthly satellite imagery from the Landsat archive with instrumental data from 1988–2012 via statistical multivariate linear modelling. Second, we used the model to extend the flooding regime record of the Marsh to the 1912–2012 period based on instrumental records of rainfall. The development of this high-resolution temporal series allowed us to explore and better understand the factors governing surface water expression in a semi-arid landscape at multiple temporal scales, and particularly the significance of extreme events. These larger temporal windows are needed to better understand long-term functioning of arid zone wetlands such as the Marsh but more broadly to establish improved context for more informed water management strategies in these sensitive regions.

2 Methods

2.1 Study site – the Fortescue Marsh

The Fortescue Marsh (hereon referred to as the Marsh; Fig. 1) is an ephemeral wetland of some 1300 km^2, which is comprised of a complex network of riverine floodplains and freshwater and floodplain lakes. The Marsh is the largest wetland of inland northwest Australia and formally recognised as nationally significant for its ecological and hydrologic values (Environment Australia, 2001; McKenzie et al., 2009; Pinder et al., 2010). Vegetation across the Marsh is dominated by salt-tolerant chenopod (*Tecticornia*) shrublands, with eucalypt and *Acacia* woodlands growing adjacent to the most permanent water features (Beard, 1975). As the largest freshwater feature for hundreds of kilometres, the Marsh (local aboriginal name *Martuyitha*) is also of considerable heritage significance including as a key focus for aboriginal communities for more than 40 000 years and since the late 1800s for early European pastoralists (Slack et al., 2009; Law et al., 2010; Barber

and Jackson, 2011).

The Marsh acts as an internally draining basin for the 31 000 km^2 upper Fortescue River catchment (21–23˚S; 119–121˚E; Fig. 1), which is physiographically separated from the Lower Fortescue River catchment by the Goodiadarrie Hills (> 410 m a.s.l.; www.water.wa.gov.au). The upper Fortescue River is the main drainage of the catchment, flowing north to northwest into the wetland system. However, numerous ephemeral creeks on the southern and northern flanks of the Fortescue Valley (Fig. 1) discharge to the marsh directly (www.water.wa.gov.au; Table A1). Flow in the Fortescue River is characterised as “variable, summer-dominated and extremely intermittent” (Kennard et al., 2010), and only very large rainfall events generate continuous flow, which contrasts with the normally dry stream beds of the dry season (WA Department of Water, 2014). Only one official daily stream gauging station is currently operational on the river (>100 km upstream of the Marsh). Other stations were only installed along the main creeks in two of the 13 sub-catchments of the Upper Fortescue River catchment (Fig. 1), and records did not overlap consistently in time (Table A1). Recently, sub-daily gauging stations were installed along Coondiner Creek and sections of Weeli Wolli Creek with pluviographs and used to implement stable isotope water balance models for these sub-catchments over relatively short (i.e., < 6 years) time periods (Dogramaci et al., 2015). The Ophthalmia Dam, constructed on the Fortescue River at Newman in 1981 to provide the town with drinking water, has a 32 GL capacity and receives from a relatively small and low lying fraction of the catchment (14.5%) with minimal observed impact on the riverine ecosystem at the mouth of the Marsh (Fig. 1; Payne and Mitchell, 1999).

The Fortescue River Valley paleodrainage, eroded from the Hamersley Basin sedimentary rocks, lies between the Hamersley Range in the south and the Chichester Range in the north, constituting the main topographical features of the eastern Pilbara (Dogramaci et al., 2012). The Fortescue Marsh consists of colluvial and alluvial sedimentary deposits up to ~50m developed on the top of the Oakover Formation, a sequence of younger Tertiary lacustrine carbonate, silcrete and mudstone rocks deposited in the Fortescue River Valley (Clout, 2011). The Oakover Formation is underlain by fractured dolomite and shale of the Wittenoom Formation (Clout, 2011). The recent sediments consist mainly of detrital clays, iron oxides and gypsum. The alluvial and colluvial aquifers of the Fortescue Marsh are

frequently confined by impermeable consolidated massive clays and calcrete and silcrete layers. Surface runoff is high via the steep gradients of creeks and gorges; recent tracer studies from the Weeli Wolli Creek and Coondiner Creek (Fig. 1) showed that residence time of water in the upper sections of the catchment was short (days to weeks) (Dogramaci et al., 2015). The groundwater under the Marsh is highly saline and likely developed by evaporation of floodwater and consequent recharge to underlying aquifers (Skrzypek et al., 2013). The most reported permanent water feature on the Marsh is 14 Mile Pool, located at the mouth of the upper Fortescue River; this pool does not retain water significantly diluted nor flushed by groundwater, which contrasts to other small through-flow pools in upper parts of the secondary tributaries of the catchment (Fellman et al., 2011; Skrzypek et al., 2013).

2.2 Climate and rainfall patterns

Rainfall in the Pilbara comes from troughs, monsoonal depressions, and onshore circulations (Leroy and Wheeler 2008; Risbey et al., 2009). Over the 1912–2012 historical period, the upper Fortescue River catchment received on average 290 mm yr^{-1}, of which 75% fell during the monsoonal summer (November–April) (Fig. 2a; Australian Bureau of Meteorology, www.bom.gov.au/cgi-bin/silo/cli_var/area_timeseries.pl). “Meteorologically dry” years received less than 200 mm rainfall, while “wet” years received over 300 mm (Fig. 2a), as defined by the left-skewed mode of the yearly rainfall frequency distribution (35% of all years). Scattered, small-scale storms cause daily rainfall to be highly variable among the 17 weather stations (Fig. 1a, Appendix A, Table 1) of the upper Fortescue River catchment (www.bom.gov.au/climate/data/). Evaporation is highest during the summer and generally exceeds rainfall (Skrzypek et al., 2013); average temperatures in summer range between 30–40 °C, and in winter months between 24–35 ˚C (www.bom.gov.au/climate/data/).

Heavy summer storms and tropical cyclones often generate large floods in the major river systems of the Pilbara, particularly on the coast, while winter rainfall is typically not sufficient to generate surface flows (Fig. 2; WA Department of Water, 2014). Tropical cyclones and other closed lows accounted for most of the extreme rainfall events in the northwest of Australia over the 1989–2009 period (Lavender and Abbs, 2013). Numerous

historical tracks of cyclones have been recorded in the upper Fortescue River catchment during the last century (www.bom.gov.au/cyclone/history/). When TC tracks were recorded within a 500 km radius of the Marsh, total monthly rainfall in the catchment was significantly greater (p value< 0.01) than the 1912–2012 monthly averages for no-TC months (Fig. 2b). Rain intensity during TC months was also higher (17–22 mm of rain per rain day) than in no-TC months (8–10 mm of rain per rain day). Not surprisingly, extremes in the rainfall record (defined here as exceeding the 95th and 99th percentile of all monthly total rainfall occurrences, or Ex_{95} and Ex_{99}, respectively) are linked to the occurrence of tropical cyclones. In fact, half of the months falling in the Ex95 (i.e., >104 mm rainfall $\cdot$ month^{-1}) recorded at least one TC (30 out of 60 months). Further, at least one TC occurrence was recorded for nine out of 12 months falling in the Ex_{99}, i.e., months recording 190–258 mm of rainfall.

2.3 Mapping flood history based on the Landsat archive (1988–2012)

We mapped the flood history (i.e., surface water expression) of the Marsh floodplain area (~1300 km^2; Fig. 1) between 1988 and 2012 from high-resolution (i.e., ca. two-week intervals) Landsat images that captured patterns of surface water expression (see Appendix A, Sect. A2 for details). The Marsh floodplain area is defined here as elevations below 410ma.s.l. and within the upper Fortescue River catchment (Fig. 1). Surface water features were extracted from Landsat images using an automated thresholding method in *ArcGIS* v. 9.2 and flood areas (F_A) were calculated using *Fragstats* v. 4.1 (see Appendix A, Sect. A2 for details). We calculated potential errors associated with using the pixel resolution (30 m) of Landsat images and the thresholding approach to classify surface water features (see Appendix A, Sect. A2 for details). Based on these potential errors, estimated monthly change in flood area (ΔF_A) of less than 6 km^2 should be considered with caution. However, given the scale of variation in F_A on the Marsh (ca. 0–1000 km^2, Fig. 3) this error is relatively small.

To provide further confidence in our dataset within the estimated errors we used two 40 cm resolution digital ortho-images produced from aerial photographs taken in July 2010 and April 2012 (Fortescue Metals Group Limited, Perth, Australia), and one 5 m resolution

image taken in August 2004 (Landgate, Government of Western Australia), to confirm that our flood areas mapped from Landsat images taken on similar dates (i.e., within one week of the ortho-image dates) were within 1 pixel (30 m) of the flood area visible in the ortho-images (Fig. A1a). A groundtruthing expedition in the dry season (November 2012; Fig. A1 b, c) that noted boundaries by GPS route tracking while walking along the water edge (~1–2 m distance from standing water) of the Moorimoordinia Native Well and a delineation of the inundation plume in the wet season (February 2012; Fig. A1 d) by GPS route tracking during low-altitude helicopter survey along the water plume were also conducted and confirm that our thresholding method captured standing water on the Marsh (Appendix A2).

2.4 Modelling floodplain wetting and drying events

2.4.1 Statistical model development and selection

Of the 493 Landsat images processed, only 208 images (TM & ETM) were used to build a calibration dataset for statistical modelling of hydrologic change between the 1988–2012 period (Fig. 3). Following selection of the latest observation for each month (or of the first observation of the next month if within the first week; $n = 265$), only ΔF_A between two consecutive months ($n = 232$) that were above the estimated errors were included. As a result, 160 ΔF_A values were used in the final calibration dataset. Most (70 %) ΔF_A values were calculated over a ca. month-long interval (i.e., 30±7 d), but this interval ranged from 16 to 48 days for the full calibration dataset.

We used a multiple linear regression (in *R* v. 2.11.1) to identify the main climatic drivers of ΔF_A on the Marsh and generate a predictive statistical model to reconstruct monthly ΔF_A for the last century (1912–2012). Climatic variables tested as predictors in the model included: monthly total rainfall, number of rain days, mean temperature and potential evapo-transpiration calculated from weather station records and monthly gridded datasets (see Appendix B, Table A3 for details). To account for the potential effect of system memory, we included F_A in the previous 1 to 12 months as predictors in the model. Initially, the sensitivity of each predictor was tested and only the hydroclimatic variables that were significant in explaining the variation in F_A were used in the model. The model that

provided the best fit between the predicted and observed values in the calibration set as per the coefficient of variation (R^2_{adj}) adjusted for the number of variables and the smallest root mean square error E_{RMS} was selected.

2.4.2 Validation of model and 1912–2012 reconstruction

The model's predictive accuracy was tested by both cross-validation and calculation of the E_{RMS} of prediction (E_{RMSP}). A random ten-fold cross-validation (CV) was computed using the CVlm function of the DAAG R package v. 1.16 (Maindonald and Braun, 2013). The E_{RMSP}, which indicates how well the model fits an independent subset of the data, was obtained by removing block subsets representing a third of the calibration occurrences (i.e., 1988–1997; 1998–2004; 2005–2012).

We used the modelled ΔF_A to reconstruct the total area flooded (F_A) from the earliest available instrumental data in the region, i.e., from March 1910 to December 2012. However, the value of F_A in March 1910 being unknown, the observed F_A minimum, average and maximum of the calibration period (1988–2012) were used as starting points and long-term statistics for the hydrological regime were calculated from the meeting point of the three time series, i.e., January 1912. Yearly statistics were calculated for the rain year, i.e., November–October. We used comparisons with an aerial photographic survey from 1957 (Edward de Courcy Clarke Earth Science Museum, UWA), early MSS Landsat imagery (1972–1988) and droughts/flood events reported by early surveyors and pastoralists to local newspapers (www.trove.nla.gov.au) to provide historical anchors to our 1912–2012 time series (see references in-text).

3 Results and discussion

3.1 Hydroclimatic determinants of floods and droughts

Total rainfall in the upper Fortescue River catchment (R), number of rain days (R_d) and carried-over inundated area (F_{At-1}) were the strongest hydroclimatic determinants of the monthly flooding and drying (ΔF_A) regime at the Fortescue Marsh (p value<0.001; Table

1). The high R^2_{adj} (0.79, *p* value< 0.001) indicates that the final model included the most important contributors to ΔF_A variation (Table A4). *R* alone tested independently of the other variable explained 64% of the variance ($p < 0.001$), and including R_d, improved variance explained by only 8% ($p < 0.001$). Although there is some collinearity between *R* and R_d (Table A4), we considered it important to include both hydroclimatic variables (*R* and R_d) from a mechanistic point of view, precisely because of the highly variable nature of our system. For example, in our study system, while it is common that 200 mm may fall over just two days, at other times 200 mm may fall over 28 days (www.bom.com.au). These very contrasting monthly distributions of rainfall demonstrate vastly different intensities and in turn generate quite different run-off; the dynamics of rainfall in such a highly heterogeneous climate are thus best captured by inclusion of both variables, where more R_d modulates negatively the impact of *R*. In addition, the inclusion of *R and* R_d may account to some extent for the recorded changing rainfall intensity over the century (Shi et al., 2008; Taschetto and England, 2009; Gallant and Karoly, 2010; Fierro and Leslie, 2013). The model's predictive accuracy was similar for both tests performed, i.e., the E_{RMSCV} and the best E_{RMSP} = 56 km^2 (Table A5; Fig. A3). However, the subset model used to calculate E_{RMSP}, which excluded the particularly wet and variable 1998–2004 period from the calibration period, performed the worst at reconstructing ΔF_A for the 1998–2004 verification period (R^2_{adj} = 0.64; E_{RMSP} = 86 km^2), indicating this period constituted an important range for the calibration of the model. Both other calibration models (excluding the 1988–1997 or the 2005–2012 periods) were more accurate (E_{RMSP} = 58 and 56 km^2, respectively), and the overall variance explained improved to 81 and 82% when either of these dry, less variable periods was removed from the model.

A lack of surface water is returned by the model as areas ≤ 0 km^2. The negative values (≤ 0 km^2) for 'area' can conceptually be explained as the depletion of the groundwater resources and lowering of the water table below the ground level. While our calibration period captures an exceptional range of intraseasonal and interannual variability in this extreme system, changes in the collinearity structure between highly collinear variables may occur over time and thus affect the relative contribution of the predictors and the reliability of the reconstructed estimates (Dormann et al., 2013). However, the relationship between *R* and R_d variables appears to have remained strongly linear between equivalent time periods over the reconstructed period, with only minor changes in the fit, slope and

intercept. Nevertheless, the coefficients of these variables should not be used outside the scope of this study. Mechanistically, we do not expect the mutual influence of R and R_d on surface flow, where for the same volume of rain more water flushes through the river network if it occurs over fewer rain days, to have changed drastically in the semi-arid region over the last 100 years, or at least not beyond the reported error of the model. Hence, this reconstruction should be used to examine long-term patterns of change in hydrological status and meteorological determinants as opposed to fine-grained catchment processes of recharge provided by higher spatio-temporally resolved hydrological models. For further details on the modelling statistics, refer to the Pearson correlation matrix for the modelled variables (Appendix A, Table A6) and the distribution of observed against reconstructed ΔF_A values (Appendix A, Fig. A2).

The goodness-of-fit and relatively small errors of the model provide confidence in the reconstruction starting in the early 1900s. While our calibration period captures an exceptional range of intraseasonal and interannual variability in this extreme system, changes in the collinearity structure between highly collinear variables may occur over time and thus affect the relative contribution of the predictors and the reliability of the reconstructed estimates (Dormann et al., 2013). However, the relationship between R and R_d variables appears to have remained strongly linear between equivalent time periods over the reconstructed period, with only minor changes in the fit, slope and intercept (Fig. A4). Nevertheless, the coefficients of these variables should not be used outside the scope of this study. Mechanistically, we do not expect the mutual influence of R and R_d on surface flow to have changed drastically in the semi-arid region over the last 100 years, where for the same volume of rain more water flushes through the river network if it occurs over fewer rain days, or at least not beyond the reported error of the model. Hence, this reconstruction should be used to examine long-term patterns of change in hydrological status and meteorological determinants as opposed to fine-grained catchment processes of recharge provided by higher spatio-temporally resolved hydrological models. However, the model tended to underestimate ΔF_A following very intense rainfall events (large rainfall over 1–3 days), which might be partly attributed to the monthly resolution (Appendix A, Fig. A2). Reconstructed values of ΔF_A for any given month are calculated for the last day of the month and as such do not account for the timing of intense events during that month. A large rainfall event that occurred early in a month would thus result in smaller ΔF_A than a

large rainfall event that occurred later in a month. The underestimation of ΔF_A values during intense events might also be due to the high spatial heterogeneity of rainfall in the catchment, which was readily apparent when events were much larger closer to the Marsh (e.g., Marillana Station, Fig. 1b; www.bom.gov.au/climate/data/). Consequently, our time series mostly reflects regional-scale events rather than more localised events. The use of weighted contributions of the different meteorological stations or sub-catchments within the upper Fortescue River catchment might improve the downscaling of this model. However, the instrumental records in this region are both temporally and spatially patchy, and using higher resolution gridded data would not necessarily truly improve the resolution of the data evenly for the last century (Fig. 1; www.bom.gov.au/climate/data/).

Severe and intense rainfall events (i.e., high R and low R_d) clearly drive the hydrologic regime of this system over the last century. Total rainfall contributed most (R_β = 145 km^2; p value < 0.001) to monthly flooding of the Marsh (ΔF_A). More than 75mm rain · month^{-1} in the catchment systematically caused a net wettening (increase in F_A) of the Marsh's floodplains while $<$30 mm rain month^{-1} was generally insufficient to impact on F_A (Fig. 4). However, more intense rainfall events resulted in much larger flooding episodes. Conversely, for the same total rainfall, more rain days in the month strongly dampened the extent of floods ($R_{d\beta}$ = –63 km^2; p value$<$ 0.001). These "flash floods" drive the current hydrological regime of the Marsh but are also consistent with the hydrochemical evolution and modern recharge of shallow groundwater under the Marsh (Skrzypek et al., 2013). By washing down of surface salts deposited on the Marsh during previous evaporation episodes, large floods not only recharge the system, but also deliver freshwater that becomes available at the surface for extended periods of time. This heavy rainfall (as opposed to groundwater) driven system is rather unusual in the arid zone, where many wetlands are groundwater-dominated, playa-like ecosystems (Bourne and Twidale, 2010; Tweed et al., 2011). In arid zone playas, the hypersaline groundwaters from the deep aquifer are connected to surface processes and result in saline waters being exposed (Bourne and Twidale, 2010; Cendon et al., 2010). In contrast, our results support that the Fortescue Marsh is rather a paleosaline lake where vegetation can grow and surface water is largely fresh, but then eventually becomes brackish due to the concentration of solutes with time owing to evaporative losses.

The sequence of events (i.e., F_{At-1}), or the "system memory", was also an important determinant of surface water availability on the Marsh. Water loss ($-\Delta F_A$) on the Marsh from one month to the next was larger over a months after higher inundation extent ($F_{At-1} >$ 0 km^2). For example, after a large flood area increase of 560 km^2 in August 1942, the water extent decreased by 100 km^2 over the first month. In contrast, an extent of 200 km^2 in May 1912 decreased by only 50 km^2 over the first month, despite a lack of rain in both cases. Because of the negative value of the F_{At-1} coefficient, this variable was not only significant in predicting ΔF_A (Table 1), but also enabled the reconstruction of continuous values for F_A over the last 100 years from ΔF_A by accounting for the "maximum drying capacity" of the system, where F_A became otherwise progressively more negative with time. The F_A values are not just correlated with F_{At-1}, they are unevenly limited (i.e., biased) within a certain range when (F_A<0) dependent on F_{At-1}. F_{At-1} hence acts as a weighting variable to account for the size-dependent range of possible values of change in F_A. Intervals (Int) between observations (number of days over which the change was observed) did not significantly improve the fit of the model (Int_β = –8 km^2; p value= 0.07). This variable (Int) was nevertheless included in the model to account for ΔF_A values being calculated over slightly different time intervals (i.e., 30±7 d) in the calibration period and because months of the year include 28 to 31 days. This, Int acted as a constant that contributed to explaining the decrease of surface water every month. Monthly loss of surface water on the Marsh through evaporation and transpiration was reconstructed to be up to 150 km^2 (i.e., lowest ΔF_A). The most severe water losses occurred during especially dry April, May and June (i.e. <3.5 mm rainfall; Fig. 4) following very wet summers. Unsurprisingly, cumulative severe floods resulted in the longest inundation periods recorded on the Marsh, and often contributed to the following year's hydrological status. Over the 1912–2012, 32% of years had up to 400 km^2 (40% fullness) surface water expression carried over to the next year (i.e., winter to summer). In contrast, 68% of years ended with no surface water and depleted aquifers in October (Fig. 5b).

Our findings indicate that the reconstructed total area flooded at the Marsh represents an integrated ecohydrological catchment response to rainfall, which is expected from such terminal basins (Haas et al., 2011). We observed that the impact of rainfall on inundations and droughts is at least in part modulated by the high local evaporation rate (five to ten-fold greater than rainfall), which acts as a constant drying force on the surface water even

1 though temperature or potential evapotranspiration (PET) did not significantly improve the
2 fit of the model. In addition, vegetation in drylands typically shows a rapid increase in
3 productivity in the few months following a large rainfall event (e.g., Veenendaal et al.,
4 1996; McGrath et al., 2012); thus, runoff from subsequent events might be dampened
5 through enhanced physiological (plant water) use, which is in turn consistent with the
6 negative effect of F_{At-1} on flood area change (Table 1). We suggest that expected seasonal
7 and interannual variation in temperature and/or PET were thus largely accounted for
8 through the use of F_{At-1} and the constant *Interval* variables.
9
10 **3.2 Spatial and temporal patterns of inundations**
11
12 Our monthly reconstruction reveals that the floodplains of the Fortescue Marsh have had
13 extremely variable interannual severity of total flooded area (F_{Amax}) that in turn determined
14 the duration of inundations for the last century (Fig. 3). Of the last 100 years (1912–2012),
15 almost 25% were large flood years, i.e., years for which the maximum flood area (F_{Amax})
16 was over 300 km^2 (Fig. 3b). Large inundations typically occurred as a result of one to
17 three-month long flood pulses in the austral summer (February–April). As described
18 earlier, these flood pulses were mainly associated with regional hydroclimatic events such
19 as one or more TCs occurring in the austral summer (January–March), and are major
20 drivers of surface water expression at the Marsh for the last century. Following large
21 floods, some level of inundation could be maintained for over 12 months in 7% of years
22 (Figs. 6 and 7). Further, only large flood years generated substantial >0.5m depth of
23 surface water (Fig. 8a), which would also have the potential to completely submerge the
24 vast chenopod community on the Marsh (Beard, 1975). These large flood years, their
25 consequent supra-seasonal sustained inundations and their connectivity to the western
26 sections (downstream) have been relatively frequent over the last century and reflect the
27 natural variability in the hydroclimatic regime. On the other hand, >800 km^2 flood years
28 (only two in the past 100 yr, 1942 and 2000) are considered extreme, infrequent
29 disturbances, which bring exceptional volumes of freshwater to the system (Fig. 8b). The
30 most striking effect of the interannual system memory was observed between 1999 and
31 2006, the period during which inundation extent and duration on the Marsh were above
32 average and unprecedented for the last century. The longest period in the last 100 years in
33 which surface water was consistently present on the Marsh (i.e., $F_A > 0$ km^2) was from

1998 to 2002, including the largest yearly inundation for the entire century in March 2000 of ~ 1000 km^2 (Fig. 3c).

In addition to the large flooding events described above, the majority of years (70–79 %) experienced at least one month of inundation resulting from smaller floods ($F_{Amax} < 40–48$ km^2) (Figs. 6 and 7) that in turn also influenced the distribution and connectivity of surface water within the different sections of the Marsh (Fig. 6). During large or severe inundation years, the entire floodplain became initially one connected flood area (Fig. 6). Following such an event in 1934, pastoralists experienced the "Marsh becoming a [400 km^2] large lake" (Fig. 6; Aitchison, 2006). Going into the winter months, evaporation and a lack of significant input from rainfall events typically resulted in drying and progressive formation of disconnected pools mainly along the northern shore and eastern end of the Marsh (Fig. 6). Based on our 25 yr calibration period, similarly severe years resulted in spatially consistent patterns of interannual inundation during both wetting and drying phases (Fig. 6). While quite frequent, large flood years do not occur at regular intervals, conferring a poor predictability to surface water in the system. The lowest recurrence was prior to 1960, with up to 14 years between two events; post 1960, large events have occurred at intervals of seven years or less, which in turn has resulted in more severe and prolonged inundations e.g., between 1999 and 2006.

The near yearly recurrence of severe and prolonged inundations over the 1999–2006 period in our record is unprecedented relative to the previous 80 or so years and consistent with the heavier summer rainfall events observed in the region over the recent decades (e.g. Shi et al., 2008; Taschetto and England, 2009; Gallant and Karoly, 2010; Fierro and Leslie, 2013). However, rigorous analysis of periodicities would be required for the appraisal of potential multi-decadal trends in the hydrological regime a background of such high variability (e.g., Kiem et al., 2003; Kiem et al., 2004; Verdon-Kidd and Kiem, 2010; Ishak et al., 2013). In fact, future investigations and risk analyses in the region should strive to assess the potential influence of known larger-scale climatic drivers and their interactions with each other on intraseasonal and interannual hydroclimate variability in the northwest of Australia (e.g., Kiem and Frank, 2004; Pui et al., 2011; Kiem and Verdon-Kidd, 2013), such as El Niño-Southern Oscillation, the Indian Ocean dipole, the Madden Julian oscillation and the southern annular mode (Risbey et al., 2009; Fierro and

Leslie, 2013). The development and application of high-resolution proxy indicators of past hydroclimatic changes for the arid zone could also provide more robust insights on multi-decadal trends and ecosystem vulnerability to these changes (e.g., Cullen and Grierson, 2007).

3.3 Significance of predictability and persistence of drought

Our reconstruction shows that the Fortescue Marsh floodplains have more often been dry (i.e., where no surface water is evident on the Marsh, or $F_A \leq 0$ km^2) than wet over the last century (Fig. 3c). Hydrological droughts (i.e., series of consecutive months where $F_A \leq 0$ km^2) of at least one year were frequent (21 %) between 1912–2012 (Figs. 3c d, and 7). The most recent drought that persisted for more than two years occurred between 1990 and 1993 (3.2 years). In contrast, particularly extended drought periods were more frequent between the late 1930s and early 1960s, with the longest supraseasonal drought on record lasting 4.3 years (between 1961 and 1965). In such water-restricted and remote environments, early pastoralists would have been the first to notice changes in the distribution and availability of freshwater. Reports of “bad drought” on Roy Hill Station in early 1939 and winter of 1940, where “no feed” for cattle was available (Aitchison, 2006) corroborate our reconstruction. Dramatic vegetation changes were also documented on the Marsh’s floodplain during this dry period (1938–1940), which coincided shortly after with Marillana Station shifting from cattle to sheep farming (Aitchison, 2006). In our time series, this documented drought corresponded to minimal surface water ($F_{Amax} < 150$ km^2) at the Marsh due to the occurrence of only minor flood events over these years (Fig. 3c). A 20-month period between 1918 and 1919 where F_A at the Marsh was reconstructed as less than 0 km^2 in our analysis also corresponds to a report by the Roy Hill Pastoral Company, one of the main pastoralist in the upper Fortescue River catchment, as a “severe drought” causing the installation of “10 new wells” in 1919 (Dept Lands and Surveys, 1919) (Fig. 3c).

Overall, the eastern section of the Marsh experienced the least interannual variability by holding the most reliably inundated freshwater areas (Fig. 6), consistent with the presence of long-lived trees at 14 Mile Pool and Moorimoordinia Native Well (Beard, 1975). The September 1957 aerial photograph also shows these pools partially filled even though

there was little summer rain that year, also corroborating our reconstruction of a dry period at that time. These more permanent, shallow water features were restricted to the floodplains at the mouth of the upper Fortescue River and other smaller tributaries draining the steeper slopes of the Chichester Range to the north (Fig. 6). These sections have thus been under a more localised and “high” inundation frequency regime from smaller events (Thomas et al., 2011; Fig. 6). These sequential, smaller events potentially maintain refugia for aquatic populations, which may facilitate recolonisation of other parts of the Marsh following the larger, less frequent flood disturbances that in turn effectively “reset” arid zone ecosystems (Leigh et al., 2010; Stendera et al., 2012). With such spatial variation in flood frequency, we can also expect vegetation communities on the Marsh to form mosaics tightly linked to their different water requirements and tolerances, as has been seen on other floodplains such as those of the Macquarie Marshes in central-eastern Australia (Thomas et al., 2011).

4 Conclusions

We developed a reliable model to predict and characterize the surface water response of a major regional wetland to hydroclimatic variability over the last century. Our approach is readily applicable to extend the temporal record to other ephemeral water bodies. Through greater understanding of system responsiveness to regional rainfall patterns, we also now have improved capacity to assess the long-term ecohydrological functioning of arid floodplains. For example, if current rainfall trends are sustained, increased flooding of the Fortescue Marsh will prolong the inundation period in the year, the connectivity between the different parts of the Marsh and the river network and increase the carry-over for the following year. The resulting enhanced persistence may in turn affect long-term hydrochemical and ecological processes of the system, e.g., by an increase in surface water salinity.

Appendix A: Mapping the flood history

A1 Landsat archive/image selection

The flood history of the Fortescue Marsh was reconstructed using standard terrain corrected scenes for systematic radiometric and geometric accuracy (Level 1T) from the USGS EarthExplorer Landsat archive (http://earthexplorer.usgs.gov/). The Landsat archive has seasonal to monthly coverage of the Fortescue Marsh from 1972–1988 and fortnightly coverage from 1988–2012. We quantified water coverage, or total flooded area (*F*A) from a subset of 493 satellite images with the analysis of wavelengths sensitive to water reflectance (Xu, 2006), specifically the short-wave infrared (SWIR) or mid-infrared (MIR) radiation bands 5 (TM, ETM) and 3 (MSS). All image processing was conducted using ArcGIS v.9.2 and ERDAS Imagine 2011. Pixel resolution was 30m x 30m (900 m^2) for the observation period (1988–2012).

A2 Flood area delineation and error

Water features were relatively straightforward to extract using a simple automated thresholding method (Xu, 2006), owing to their very high contrast to the surrounding arid landscape. F_A could not be estimated using our automated method when partial cloud cover was present in the satellite imagery, or for the ETM-SLC off series of Landsat 7 (169 images from a total of 493). Therefore, F_A was estimated in these years by calculating the midpoint between the most recent "before and after" F_A estimates. This approach also allowed us to capture the largest F_A estimates as they were often partly obstructed by clouds.

To account for registration error across the temporal and satellite series, the F_A estimate and its associated error (*estimation errors*) were obtained from three water features extracted for every image using a lower, mid and upper threshold of reflectance values. The three consecutive threshold values (either 10, 20, 30, 40, 50, or 60 value of reflectance) were selected to include the highest frequency distribution of water pixels while providing the smallest F_A estimate error. We also calculated *resolution errors* in extracting F_A to account for the use of 30m x 30m pixels values. Here, we applied a 15m

buffer inside and outside the water-only polygon for all thresholds. Thus, *estimation* and *resolution errors* were largest when F_A was small owing to an increase in the "edge length" to size ratio, and differences in F_A less than 6 km_2 should be considered with caution. A simple linear regression obtained between the automated F_A and its buffer was used to calculate the resolution error for these shapes. The *resolution error* for shape-estimated F_A was calculated using linear regression formulas obtained between F_A and inside buffer (R_2 = 0.99, p value< 0.001) and outside buffer (R^2 = 0.99, p value< 0.001). Strong congruency between elevation contours and the shape of flooded area estimates on the Fortescue Marsh indicate that our thresholding methodology accurately detected standing water. Neither *estimation* nor *resolution errors* were found to follow a seasonal or overall temporal trend. However, we cannot discount that areas of waterlogged ground also contributed to the estimates of flooded area (Castañeda et al., 2005).

Appendix B: Climate variables

While 17 meteorological stations have been intermittently recording daily rainfall data in the upper Fortescue River catchment, only six are currently still in operation, forming a too sparse and temporally inconsistent network for direct use in this study (Fig. 1; Table A2). Explanatory hydroclimatic variables were thus generated using monthly gridded datasets resolved at either 0.5 or 1˚ cell size weighted for their relative contribution to the upper Fortescue River catchment (Table A3). Total rainfall and mean temperature were obtained from the Australian Bureau of Meteorology (www.bom.gov.au/cgi-bin/silo/cli_var/area_timeseries.pl), the Climatic Research Unit (CRU) and the Global Precipitation Climatology Centre (GPCC) via the Koninklijk Nederlands Meteorologisch Instituut (KNMI) Climate Explorer (climexp.knmi.nl). Potential evapotranspiration (PET), calculated using Penman–Monteith parameterization and based on the actual vegetation cover, was from van der Schrier et al. (2013). The mean number of rain days · $month^{-1}$ (R_d) was calculated from daily rainfall records obtained from the four meteorological stations still in operation, located within or close to the upper Fortescue River catchment, relatively evenly distributed across the vast geographic area and with the longest records (i.e., Noreena Downs, Bulloo Downs, Marillana and Mulga Downs) (Fig. 1; Table A2).

Author contributions. A. Rouillard wrote the paper with input from P. F. Grierson, G. Skrzypek, C. Turney and S. Dogramaci. A. Rouillard collected and processed the satellite imagery and conducted the statistical analyses. A. Rouillard and G. Skrzypek developed the modelling approach after discussion with co-authors. The study was conceived by P. F. Grierson, A. Rouillard, G. Skrzypek, S. Dogramaci and C. Turney.

Acknowledgements. We thank the two anonymous referees and the Editors for their constructive comments, which have helped focus and improve the quality of the manuscript. This research was supported by the Australian Research Council (ARC) in partnership with Rio Tinto (LP120100310). A. Rouillard was supported by the Australian Government and UWA via an International Postgraduate Research Scholarships (IPRS) and an Australian Postgraduate Awards (APA), as well as by the Canadian and Québec governments via a Natural Sciences and Engineering Research Council (NSERC) and a Fonds québécois de la recherche sur la nature et les technologies (FQRNT) via graduate scholarships. G. Skrzypek participation is supported by an ARC Future Fellowship (FT110 100 352). We thank the Fortescue Metals Group Ltd for access to ortho-images and Digital Elevation Model of the Fortescue Marsh. The authors thank Jeremy Wallace (CSIRO) and Victoria Marchesini (UWA) for advice on image processing, Gerard van der Schrier (KNMI) for sharing the PET dataset, Gavan McGrath (UWA) for council on tropical cyclones, Caroline Bird (Archae-Aus) for help with archival research and the following researchers for their assistance with the modelling: Yun Li (CSIRO), Jérôme Chopard (UWA), Michael Renton (UWA), Edward Cook (UColumbia), Jonathan Palmer (UTAS) and Jason Smerdon (UColumbia). We also acknowledge the kind support of Lee and Sue Bickell (Marillana Station), Barry and Bella Gratte (Ethel Creek Station), Victor and Larissa Gleeson (Mulga Downs Station), and Murray and Ray Kennedy (Roy Hill Station). We are also grateful to Alison O'Donnell and Gerald Page for providing useful comments on the early and final versions of the manuscript.

References

Aitchison, G. P.: “I’ve Had a Good Life” Phil’s Story: The Autobiography of a Pilbara Pioneer, Western Australia, Hesperian Press, Carlisle, 48 pp., 2006.

Bai, J., Chen, X., Li, J., Yang, L., and Fang, H.: Changes in the area of inland lakes in arid regions of central Asia during the past 30 years, Environ. Monit. Assess., 178, 247–256, 2011.

Barber, M. and Jackson, S.: Water and Indigenous People in the Pilbara, Western Australia: a Preliminary Study, CSIRO: Water for a Healthy Country Flagship Report, Darwin, 104 pp., 2011.

Bates, P. D.: Integrating remote sensing data with flood inundation models: how far have we got?, Hydrol. Process., 26, 2515–2521, 2012.

Beard, J. S.: The Vegetation of the Pilbara Area, Vegetation Survey of Western Australia, 1: 1000000 Vegetation Series, Map and Explanatory Notes, The University of Western Australia Press, Nedlands, 1975.

Bourne, J. A. and Twidale, C. R.: Playas of inland Australia, Cad. Lab. Xeol. Laxe, 35, 71–97, 2010.

Box, J. B., Duguid, A., Read, R. E., Kimber, R. G., Knapton, A., Davis, J., and Bowland, A. E.: Central Australian waterbodies: the importance of permanence in a desert landscape, J. Arid Environ., 72, 1395–1413, 2008.

Castaneda, C., Herrero, J., and Auxiliadora, C., M.: Landsat monitoring of playa-lakes in the Spanish Monegros desert, J. Arid Environ., 63, 497–516, 2005.

Cendon, D. I., Larsen, J. R., Jones, B. G., Nanson, G. C., Rickleman, D., Hankin, S. I., Pueyo, J. J., and Maroulis, J.: Freshwater recharge into a shallow saline groundwater system,

Cooper Creek floodplain, Queensland, Australia, J. Hydrol., 392, 150–163, 2010.

Clout, J. M. F.: The Roy Hill Project, AisIMM, 3, 52–65, 2011.

Cullen, L. E. and Grierson, P. F.: A stable oxygen, but not carbon, isotope chronology of Callitris columellaris reflects recent climate change in north-western Australia, Clim. Change, 85, 213–229, 2007.

Department of Land and Survey: “Surveys by Roy Hill Pastoral Co in Victoria district of Roy Hill Station”, ACC541, file 5125, Archive Collection of the State Records Office of Western Australia, 1919.

Dogramaci, S., Firmani, G., Hedley, P., Skrzypek, G., and Grierson, P.F.: Evaluating recharge to an ephemeral dryland stream using a hydraulic model and water, chloride and isotope mass balance, Journal of Hydrology, 521, 520–532, 2015.

Dogramaci, S., Skrzypek, G., Dodson, W., and Grierson, P. F.: Stable isotope and hydrochemical evolution of groundwater in the semi-arid Hamersley Basin of subtropical northwest Australia, J. Hydrol., 475, 281–293, 2012.

Dormann, C.F., Elith, J., Bacher, S., Buchmann, C., Carl, G., Carré, G., García Marquéz, J.R., Gruber, B., Lafourcade, B., Leitão, P.J., Münkemüller, T., McClean, C., Osborne, P.E., Reineking, B., Schröder, B., K. Skidmore, A., Zurell, D., and Lautenbach, S.: Collinearity: a review of methods to deal with it and a simulation study evaluating their performance, Ecography, 36, 27–46, 2013.

Environment Australia: A Directory of Important Wetlands in Australia, 3rd Edn., Environment Australia, Canberra, Australia, 157 pp., 2001.

Fierro, A.O., and Leslie, L.M.: Links between Central West Western Australian Rainfall Variability and Large-Scale Climate Drivers, J. Clim., 26, 2222–2245, 2013.

Fellman, J. B., Dogramaci, S., Skrzypek, G., Dodson, W., and Grierson, P. F.: Hydrologic control of dissolved organic matter biogeochemistry in pools of a subtropical dryland river, Water Resour. Res., 47, 1–13, 2011.

Feng, X., Porporato, A., and Rodriguez-Iturbe, I.: Changes in rainfall seasonality in the tropics, Nat. Clim. Change, 3, 811–815, 2013.

Gallant, A. J. E. and Karoly, D. J.: A combined climate extremes index for the Australian region, B. Am. Meteorol. Soc., 23, 6153–6165, 2010.

Gardelle, J., Hiernaux, P., Kergoat, L., and Grippa, M.: Less rain, more water in ponds: a remote sensing study of the dynamics of surface waters from 1950 to present in pastoral Sahel (Gourma region, Mali), Hydrol. Earth Syst. Sci., 14, 309–324, doi:10.5194/hess-14-309-2010, 2010.

Geoscience Australia (GA): 1 Second SRTM Derived Hydrological Digital Elevation Model (DEM-H) Version 1.0, Commonwealth of Australia, 2011.

Haas, E. M., Bartholomé, E., Lambin, E. F., and Vanacker, V.: Remotely sensed surface water extent as an indicator of short-term changes in ecohydrological processes in sub-Saharan Western Africa, Remote Sens. Environ., 115, 3436–3445, 2011.

Harms, T. K. and Grimm, N. B.: Influence of the hydrologic regime on resource availability in a semi-arid stream-riparian corridor, Ecohydrology, 3, 349–359, 2010.

Ishak, E.H., Rahman, A., Westra, S., Sharma, A., and Kuczera, G.: Evaluating the non-stationarity of Australian annual maximum flood, J. Hydrol., 494, 134–145, 2013.

Karim, F., Kinsey-Henderson, A., Wallace, J., Arthington, A. H., and Pearson, R. G.: Modelling wetland connectivity during overbank flooding in a tropical floodplain in north Queensland, Australia, Hydrol. Process., 26, 2710–2723, 2012.

Kennard, M. J., Pusey, B. J., Olden, J. D., Mackay, S. J., Stein, J. L., and Marsh, N.: Classification of natural flow regimes in Australia to support environmental flow management, Freshwater Biol., 55, 171–193, 2010.

Kiem, A.S., Franks, S.W., and Kuczera, G.: Multi-decadal variability of flood risk, Geophys. Res. Lett., 30, 1–4, 2003.

Kiem, A.S., and Franks, S.W.: Multi-decadal variability of drought risk, eastern Australia, Hydrol. Proc., 18, 2039–2050, 2004.

Kiem, A.S., and Verdon-Kidd, D.C.: The importance of understanding drivers of hydroclimatic variability for robust flood risk planning in the coastal zone, Aust. J. Wat. Res., 17, 126, 2013.

Lavender, S. L. and Abbs, D. J.: Trends in Australian rainfall: contribution of tropical cyclones and closed lows, Clim. Dynam., 40, 317–326, 2013.

Law, W. B., Cropper, D. N., and Petchey, F.: Djadjiling rockshelter: 35,000 14C years of Aboriginal occupation in the Pilbara, western Australia, Aust. Archaeol., 70, 68–71, 2010.

Leigh, C., Sheldon, F., Kingsford, R. T., Arthington, A. H.: Sequential floods drive “booms” and wetland persistence in dryland rivers: a synthesis, Mar. Freshwater Res., 61, 896–908, 2010.

Maindonald, J. and Braun, W. J.: DAAG: Data Analysis And Graphics data and functions, available at: www.stats.uwo.ca/DAAG/, 2013.

McCarthy, J. M., Gumbricht, T., McCarthy, T., Frost, P., Wessels, K., and Seidel, F.: Flooding patterns of the Okavango wetland in Botswana between 1972 and 2000, Ambio, 32, 453–457, 2003.

McGrath, G. S., Sadler, R., Fleming, K., Tregoning, P., Hinz, C., and Veneklaas, E. J.: Tropical cyclones and the ecohydrology of Australia's recent continental-scale drought, Geophys. Res. Lett., 39, 1–6, 2012.

McKenzie, N. L., van Leeuwen, S., and Pinder, A. M.: Introduction to the Pilbara biodiversity survey, 2002–2007, Records of the Western Australian Museum, Supplement, 78, 3–89, 2009.

Mori, A. S.: Ecosystem management based on natural disturbances: hierarchical context and non-equilibrium paradigm, J. Appl. Ecol., 48, 280–292, 2011.

Neal, J., Schumann, G., and Bates, P.: A subgrid channel model for simulating river hydraulics and floodplain inundation over large and data sparse areas, Water Resour. Res., 48, 1–16, 2012.

Newman, B. D., Wilcox, B. P., Archer, S. R., Breshears, D. D., Dahm, C. N., Duffy, C. J., McDowell, N. G., Phillips, F. M., Scanlon, B. R., and Vivoni, E. R.: Ecohydrology of water-limited environments: a scientific vision, Water Resour. Res., 42, 1–15, 2006.

Payne, A. L. and Mitchell, A. A.: An Assessment of the Impact of Ophthalmia Dam on the Floodplains of the Fortescue River on Ethel Creek and Roy Hill Stations, Resource Management Technical Report No. 124, Western Australian Department of Agriculture, Perth, Western Australia, 60 pp., 1999.

Pinder, A. M., Halse, S. A., Shiel, R. J., and McRae, J. M.: An arid zone awash with diversity: patterns in the distribution of aquatic invertebrates in the Pilbara region of Western Australia, Records of the Western Australian Museum, 78, 205–246, 2010.

Powell, S. J., Letcher, R. A., and Croke, B. F. W.: Modelling floodplain inundation for environmental flows: Gwydir wetlands, Australia, Ecol. Model., 211, 350–362, 2008.

Pui, A., Lal, A., and Sharma, A.: How does the Interdecadal Pacific Oscillation affect design floods in Australia?, Water Resources Research, 47, W05554, 1–13, 2011.

Risbey, J. S., Pook, M. J., McIntosh, P. C., Wheeler, M. C., and Hendon, H. H.: On the remote drivers of rainfall variability in Australia, Mon. Weather Rev., 137, 3233–3253,

2009.

Roshier, D. A., Whetton, P. H., Allan, R. J., and Robertson, A. I.: Distribution and persistence of temporary wetland habitats in arid Australia in relation to climate, Austral Ecol., 26, 371–384, 2001.

Schrier, G., Barichivich, J., Bri⬥a, K. R., and Jones, P. D.: A scPDSI-based global data set of dry and wet spells for 1901–2009, J. Geophys. Res.-Atmos., 118, 4025–4048, 2013.

Shi, G., Ribbe, J., Cai, W., and Cowan, T.: An interpretation of Australian rainfall projections, Geophys. Res. Lett., 35, 1–6, 2008.

Skrzypek, G., Dogramaci, S., and Grierson, P. F.: Geochemical and hydrological processes controlling groundwater salinity of a large inland wetland of northwest Australia, Chem. Geol., 357, 164–177, 2013.

Slack, M., Fillios, M., and Fullagar, R.: Aboriginal settlement during the LGM at Brockman, Pilbara region, Western Australia, Archaeol. Ocean., 44, 32–39, 2009.

Sponseller, R. A., Heffernan, J. B., and Fisher, S. G.: On the multiple ecological roles of water in river networks, Ecosphere, 4, 17, 1–4, 2013.

Stendera, S., Adrian, R., Bonada, N., Cañedo-Argüelles, M., Hugueny, B., Januschke, K., Pletterbauer, F., and Hering, D.: Drivers and stressors of freshwater biodiversity patterns across different ecosystems and scales: a review, Hydrobiologia, 696, 1–28, 2012.

Taschetto, A. S. and England, M. H.: An analysis of late twentieth century trends in Australian rainfall, Int. J. Climatol., 29, 791–807, 2009.

Thomas, R. F., Kingsford, R. T., Lu, Y., and Hunter, S. J.: Landsat mapping of annual inundation (1979–2006) of the Macquarie Marshes in semi-arid Australia, Int. J. Remote Sens., 32, 4545–4569, 2011.

Trigg, M. A., Michaelides, K., Neal, J. C., and Bates, P. D.: Surface water connectivity dynamics of a large scale extreme flood, J. Hydrol., 505, 138–149, 2013.

Tweed, S., Leblanc, M., Cartwright, I., Favreau, G., and Leduc, C.: Arid zone groundwater recharge and salinisation processes; an example from the Lake Eyre Basin, Australia, J. Hydrol., 408, 257–275, 2011.

van Etten, E. J. B.: Inter-annual rainfall variability of arid Australia: greater than

elsewhere?, Aust. Geogr., 40, 109–120, 2009.

Veenendaal, E. M., Ernst, W. H. O., and Modise, G. S.: Effect of seasonal rainfall pattern on seedling emergence and establishment of grasses in a savanna in south-eastern Botswana, J. Arid Environ., 32, 305–317, 1996.

Verdon-Kidd, D.C., and Kiem, A.S.: Nature and causes of protracted droughts in southeast Australia: Comparison between the Federation, WWII, and Big Dry droughts, Geophys. Res. Lett., 36, 1–6, 2009.

Viles, H. A. and Goudie, A. S.: Interannual, decadal and multidecadal scale climatic variability and geomorphology, Earth-Sci. Rev., 61, 105–131, 2003.

Wen, L., Macdonald, R., Morrison, T., Hameed, T., Saintilan, N., and Ling, J.: From hydrodynamic to hydrological modelling: investigating long-term hydrological regimes of key wetlands in the Macquarie Marshes, a semi-arid lowland floodplain in Australia, J. Hydrol., 500, 45–61, 2013.

Western Australia (WA) Department of Water: 708011: Foretescue River – Newman, River Monitoring Stations in Western Australia, available at: www.kumina.water.wa.gov.au/waterinformation/wir/reports/publish/708011/708011 (last access: 7 October 2014), 2014.

White, P. S. and Pickett, S. T. A. Natural disturbance and patch dynamics: an introduction, in: The Ecology of Natural Disturbance and Patch Dynamics, edited by: Pickett, S. T. A. and White, P. S. Academic Press, Orlando, USA, 3–16, 1985.

Water INformation (WIN) database—discrete sample data. [21 May 2014]. Department of Water, Water Information section, Perth Western Australia.

Xu, H.: Modification of normalised difference water index (NDWI) to enhance open water features in remotely sensed imagery, Int. J. Remote Sens., 27, 3025–3033, 2006.

Table 1: Model parameter estimates and standardised statistics for the final linear model to reconstruct historical flood area on the Fortescue Marsh, NW Australia

Driver	β (km^2)	Effect	p value
R	144.729	+	< 0.001
R_d	–62.950	–	< 0.001
F_{At-1}	–29.157	±	< 0.001
Int	–7.650	–	0.070
Intercept	–8.040	–	0.816

Note: β = Weighted contribution; Effect = gain (+) or loss (−) effect of each variable on change in flood area (ΔF_A); R = total rainfall · month^{-1} on the upper Fortescue; R_d = number of days with > 0 mm of rain · month^{-1}; F_{At-1} = flood area of the previous month; Int = the time interval between observations; Intercept = equation intercept

Table A1: Temporal coverage of all official stream gauging stations in the Upper Fortescue River catchment and maximum recorded daily discharge

Site number	Stream Name	Name	Operational date	Last measurement	Max discharge (m^3 sec^{-1})	Total discharge (GL)
708001	Marillana Ck	Flat Rocks	15/08/1967	23/02/1983	1327	72
708006	Fortescue River	Goodiadarrie Crossing	01/12/1972	01/10/1986	*	*
708008	Fortescue River	Roy Hill	01/09/1973	29/09/1986	*	*
708011	Fortescue River	Newman	09/01/1980	Present	1730	78
708013	Weeli Wolli Ck	Waterloo Bore	30/11/1984	Present	4137	142
708014	Weeli Wolli Ck	Tarina	10/05/1985	Present	2100	62
708016	Weeli Wolli Ck	Weeli Wolli Springs	08/10/1997	14/07/2008	423	10

Note: * Only daily stage height available; location of stations marked on Fig. 1

Table A2: Australian Bureau of Meteorology (BoM) rainfall stations (www.bom.gov.au/climate/data/) located within and nearby the upper Fortescue River catchment, NW Australia.

No	Station name	BoM number	Lat (˚N)	Long (˚E)	Status	Year open	Year closed
	Mulga Downs	5015	−22.10	118.47	Open	1898	
	Bulloo Downs	7019	−24.00	119.57	Open	1917	
	Marillana	5009	−22.63	119.41	Open	1936	
	Noreena Downs	4026	−22.29	120.18	Open	1911	
1	Balfour Downs	4003	−22.80	120.86	Closed	1907	1998
2	Wittenoom	5026	−22.24	118.34	Open	1949	
3	Auski Munjina Roadhouse	5093	−22.38	118.69	Open	1998	
4	Kerdiadary	5047	−22.25	119.10	Closed	1901	1910
5	Warrie	5025	−22.40	119.53	Closed	1927	1964
6	Bonney Downs	4006	−22.18	119.94	Open	1907	
7	Poondawindie	4063	−22.20	120.20	Closed	1930	1938
8	Sand Hill	5064	−22.78	119.62	Closed	1971	1984
9	Roy Hill	5023	−22.62	119.96	Closed	1900	1998
10	Ethel Creek	5003	−22.90	120.17	Closed	1907	2003
11	Packsaddle Camp	5089	−22.90	118.70	Closed	1989	2002
12	Rhodes Ridge	7169	−23.10	119.37	Open	1971	
13	Rpf 672 Mile	4065	−22.70	121.10	Closed	1913	1947
14	Billinnooka	13029	−23.03	120.90	Closed	1960	1974
15	Jigalong	13003	−23.36	120.78	Closed	1913	1991
16	Minderoo	7172	−23.40	119.78	Closed	1913	1931
17	Newman Aero	7176	−23.42	119.80	Open	1971	
18	Capricorn Roadhouse	7191	−23.45	119.80	Open	1975	
19	Murramunda	7102	−23.50	120.50	Closed	1915	1949
20	Sylvania	7079	−23.59	120.05	Open	1950	
21	Prairie Downs	7153	−23.55	119.15	Open	1968	
22	Turee Creek	7083	−23.62	118.66	Open	1920	
23	Mundiwindi	7062	−23.79	120.24	Closed	1915	1981
24	Rpf 561 Mile	13013	−23.90	120.40	Closed	1913	1947
	Newman	7151	−23.37	119.73	Closed	1965	2003

Note: * Numbers correspond to location of stations marked on Fig. 1

Table A3: Climate variables used in the development of a linear model to reconstruct historical flood area on the Fortescue Marsh, NW Australia.

Interval	Variable	Res.	Location	Period	Source
d	*R*		Bulloo Downs	1917–2012	www.bom.gov.au/climate/data/
d	*R*		Marillana	1936–2012	www.bom.gov.au/climate/data/
d	*R*		Mulga Downs	1907–2012	www.bom.gov.au/climate/data/
d	*R*		Noreena Downs	1911–2012	www.bom.gov.au/climate/data/
m	*R*	1˚	UF	1900–2012	www.bom.gov.au/cgi-bin/silo/cli_var/area_timeseriespl
m	*R*	0.5˚	UF	1901–2012	GPCC V6 rain gauge precipitation dataset
m	*R*	0.5˚	UF	1901–2009	CRU time-series (TS) version 3.10.01 (land)
m	*T*	1˚	UF	1910–2012	www.bom.gov.au/cgi-bin/silo/cli_var/area_timeseriespl
m	*T*	0.5˚	UF	1901–2009	CRU TS 3.10 (land)
m	PET	0.5˚	UF	1901–2009	(Schrier et al., 2013)

Note: Res. stands for the resolution of gridded data, d is daily weather station rainfall data, m is monthly gridded climate data, *R* is total rainfall (mm), *T* is mean temperature (°C) and PET is Penman-Monteith potential evapotranspiration index. *UF* is the upper Fortescue River catchment (31,000 km^2).

Table A4: Sensitivity analysis of the four variables included in the statistical model

Final	Model											
	R^2_{adj}	0.79										
	p	<0.001										
	E_{RMS}	52										
	Driver	Coeff	Error	*p*								
	R	2.9	0.2	<0.001								
	R_d	−18.8	2.4	<0.001								
	F_{At-1}	−0.13	0.02	<0.001								
	Int	−0.99	0.54	0.070								
	Intercept	4.3	18.3	0.816								
1-variable	Model											
	R^2_{adj}	0.64			0.28							
	p	<0.001			<0.001							
	E_{RMS}	68			96							
	Driver	Coeff	Error	*p*	Coeff	Error	*p*					
	R	1.86	0.11	<0.001	-	-	-					
	R_d	-	-	-	18.29	2.29	<0.001					
	F_{At-1}	-	-	-	-	-	-					
	Int	-	-	-	-	-	-					
	Intercept	−67.158	6.42	<0.001	−58.351	9.898	<0.001					
4-variable	Model											
	R^2_{adj}	0.35			0.71			0.72			0.79	
	p	<0.001			<0.001			<0.001			<0.001	
	E_{RMS}	91			61			59			52	
	Driver	Coeff	Error	*p*	Coeff	Error	*p*	Coeff	Error	*p*	Coeff	Error	*p*
	R	-	-	-	1.8	0.1	<0.001	3.0	0.2	<0.001	2.9	0.2	<0.001
	R_d	18.0	2.2	<0.001	-	-	-	−18.8	2.7	<0.001	−18.4	2.4	<0.001
	F_{At-1}	−0.14	0.03	<0.001	−0.13	0.02	<0.001	-	-	-	−0.13	0.02	<0.001
	Int	0.18	0.94	0.847	−0.57	0.63	0.370	−0.93	0.62	0.133	-	-	-
	Intercept	−39.6	31.9	0.216	−26.0	21.1	0.220	−20.8	20.5	0.311	−27.1	6.4	<0.001

Note: *R* = total rainfall·month^{-1} on the upper Fortescue (mm); R_d = number of days with > 0 mm of rain·month^{-1} (days); F_{At-1} = flood area of the previous month (km^2); *Int* = the time interval between observations (days); Std Error = Standard error; *p* = significance level

Table A5: Analysis of predictive accuracy of the final model based on the full 1988–2012 calibration period and the subsets for the 1998–2012, 1988–1997; 2005–2012, 1988–2004 periods.

Period	1988–2012			1998–2012			1988–1997; 2005–2012			1988–2004		
R^2_{adj}	0.79			0.82			0.64			0.81		
p	<0.001			<0.001			<0.001			<0.001		
E_{RMS}	52			51			46			56		
E_{RMSP}	-			58			86			56		
Driver	Coeff	Error	p	Coeff	Error	p	Coeff	Error	p	Coeff	Error	p
R	2.9	0.2	<0.001	2.9	0.2	<0.001	2.1	0.2	<0.001	3.3	0.2	<0.001
R_d	−18.8	2.4	<0.001	−17.7	2.6	<0.001	−10.7	3.0	<0.001	−24.0	3.4	<0.001
F_{At-1}	−0.13	0.02	<0.001	−0.13	0.02	<0.001	−0.17	0.03	<0.001	−0.12	0.02	<0.001
Int	−0.99	0.54	0.070	−0.73	0.71	0.874	−1.24	0.61	0.044	−1.02	0.67	0.134
Intercept	4.3	18.3	0.816	−3.7	23.4	0.305	15.3	20.9	0,467	4.3	23.0	0.853

Note: R = total rainfall·month^{-1} on the upper Fortescue (mm); R_d = number of days with > 0 mm of rain·month^{-1} (days); F_{At-1} = flood area of the previous month (km^2); *Int* = the time interval between observations (days); Std Error = Standard error; p = significance level

Table A6: Pearson correlation matrix of the variables included in the final linear model to reconstruct historical flood area on the Fortescue Marsh, NW Australia

	R	R_d	F_{At-1}	Int
R	1	-	-	-
R_d	0.8518 p<0.001	1	-	-
F_{At-1}	−0.0361 p=0.6507	−0.0313 p=0.6943	1	-
Int	0.0703 p=0.3767	0.0089 p=0.9108	−0.0162 p= 0.8388	1

Note: R = total rainfall·month^{-1} on the upper Fortescue (mm); R_d = number of days with > 0 mm of rain·month^{-1} (days); F_{At-1} = flood area of the previous month (km^2); Int = the time interval between observations (days)

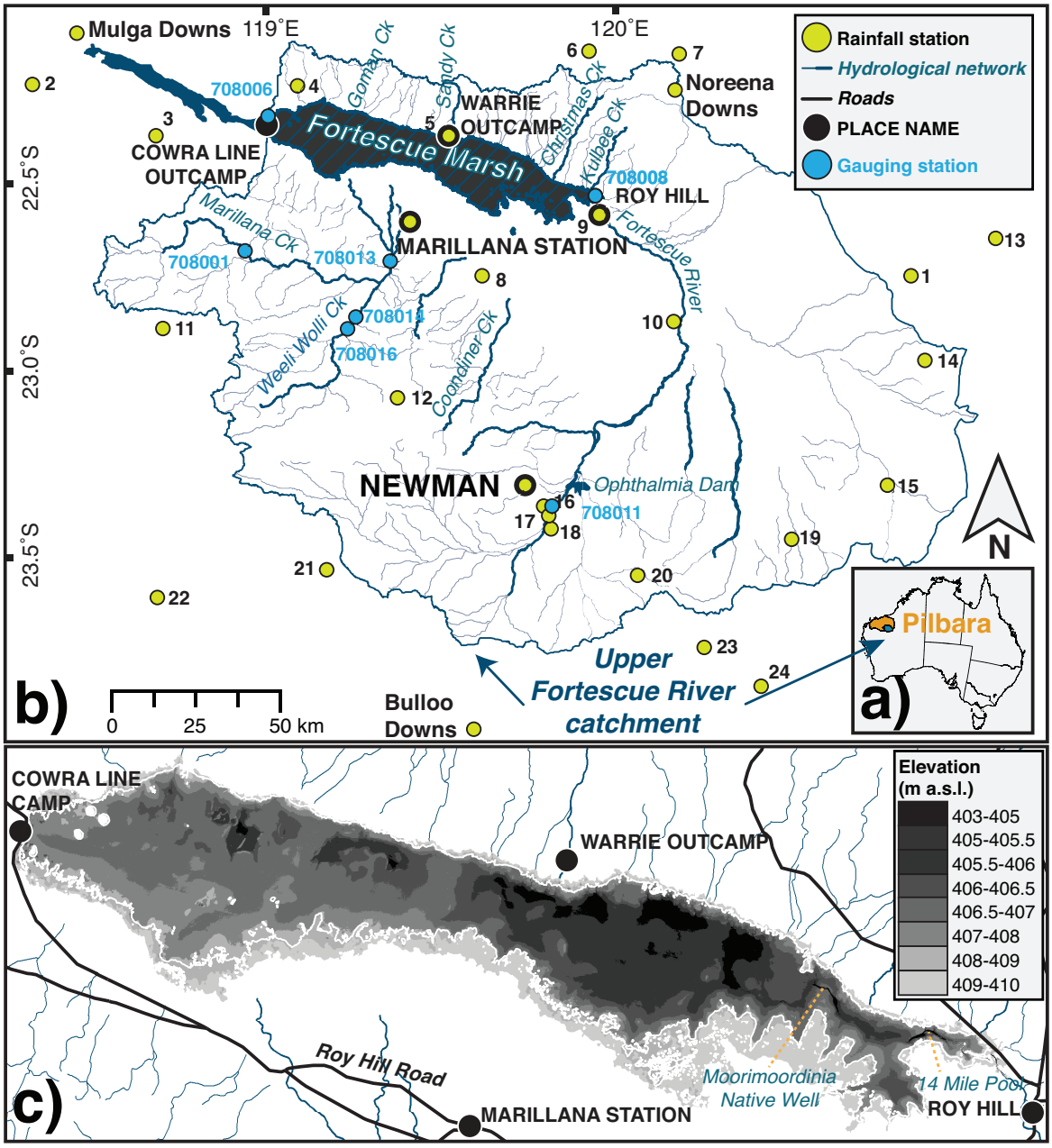

Figure 1: The **a)** Pilbara region in northwest Australia, **b)** Upper Fortescue River catchment and river network (blue lines; DoW, 2014), including the Fortescue Marsh's floodplain area used in this study (black hatched section; < 410 m a.s.l. extracted from a 1 sec DEM-H, Geoscience Australia, 2011), stream gauging stations (blue circles, see full list in Appendix A, Table A1; WIN, 2014) and meteorological stations (green circles, see full list in Appendix A, Table A2; www.bom.gov.au/climate/data/) and **c)** elevation of the study area (0.1 m vertical accuracy (RMS) LiDAR Survey DEM; Fortescue Metals Group Ltd, 2010) with roads and place name (black lines and circles; Geoscience Australia, 2001). *Generated in ArcMap v. 9.2.*

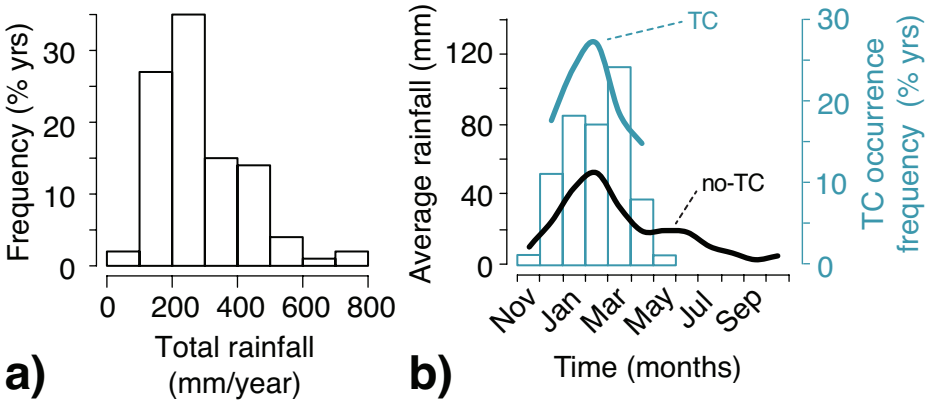

Figure 2: The upper Fortescue River catchment 1912–2012 hydroclimate with **a)** frequency distribution of total yearly rainfall and **b)** average monthly rainfall for months recording at least one tropical cyclone (TC) within 500 km radius of the upper Fortescue River catchment (blue line) and without TC recorded (black line), with the number of years (frequency) where TC occurrence was recorded for each month of the water year (blue columns); only one occurrence of TC was recorded in Nov and May for the last century and thus rainfall averages for these months were not included. Source: www.bom.gov.au/cgi-bin/silo/cli_var/area_timeseriespl & www.bom.gov.au/cyclone/history/.

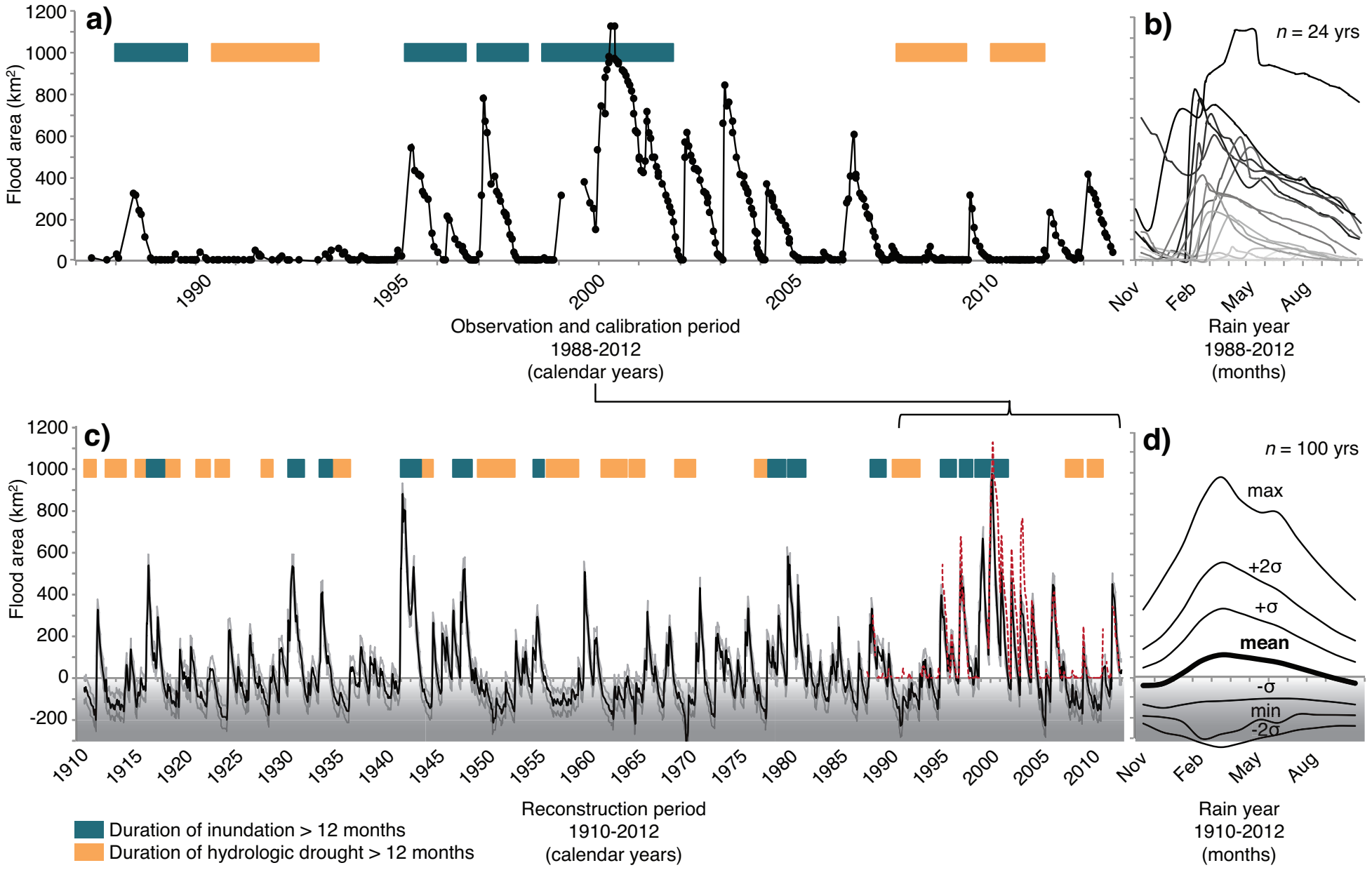
a)
b)
c)
d)
Flood area (km²)
1200
1000
800
600
400
200
0
-200
1990
1995
2000
2005
2010
1910
1915
1920
1925
1930
1935
1940
1945
1950
1955
1960
1965
1970
1975
1980
1985
1990
1995
2000
2005
2010
n = 24 yrs
n = 100 yrs
Nov
Feb
May
Aug
max
+2σ
+σ
mean
-σ
min
-2σ
Observation and calibration period
1988-2012
(calendar years)
Rain year
1988-2012
(months)
Reconstruction period
1910-2012
(calendar years)
Rain year
1910-2012
(months)
Duration of inundation > 12 months
Duration of hydrologic drought > 12 months

Figure 3: 1988–2012 **a)** flood area observation and calibration dataset (solid black line with dots for each observation) and its **b)** timing of seasonal change over the rain year (n = 24 yr); 1912–2012 **c)** flood area reconstruction (solid black line), monthly E_{RMSP} of ΔF_A = ±56 km^2 (solid grey lines) and observation dataset plotted for the 1988–2012 period (red dashed line) for comparison and **d)** monthly mean, minimum (min), maximum (max) and 1 and 2 σ ranges of variation over the rain year for the reconstructed period (n = 100 yr). Overlaid on **a)** and **c)** time-series are the supraseasonal dry and wet periods, where F_A was either < 0 km^2 or > 0 km^2 for over 12 consecutive months. c) & d) $F_A \leq 0$ km^2 = no surface water evident on the Marsh (shaded).

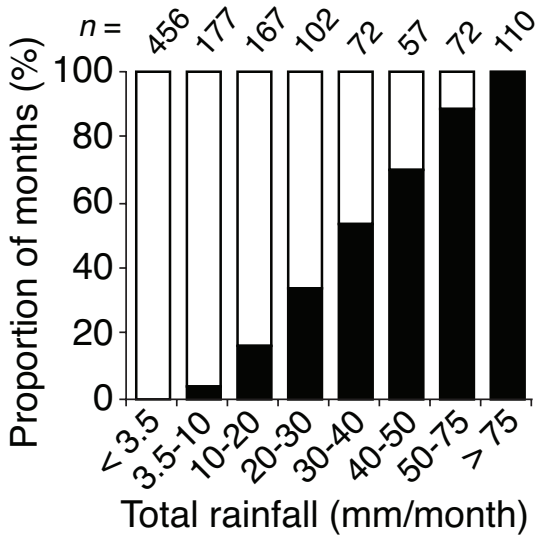

Figure 4: Total monthly rainfall in the upper Fortescue River catchment (Total rainfall) causing an increase in surface water area measured as the proportion of months with net change in flood area or $\Delta F_A > 0$ km^2 (black columns) at the Fortescue Marsh (1912–2012).

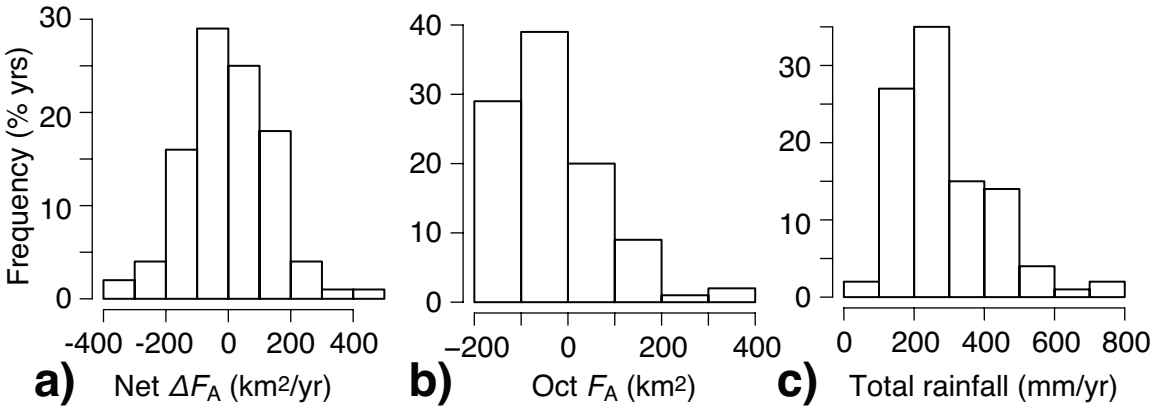

Figure 5: 1912–2012 frequency distributions of yearly **a)** net change in flood area (ΔF_A), **b)** end-of-the-year flood area (Oct F_A) and **c)** yearly maximum flood area (F_{Amax}; km^2), n = 100 yr.

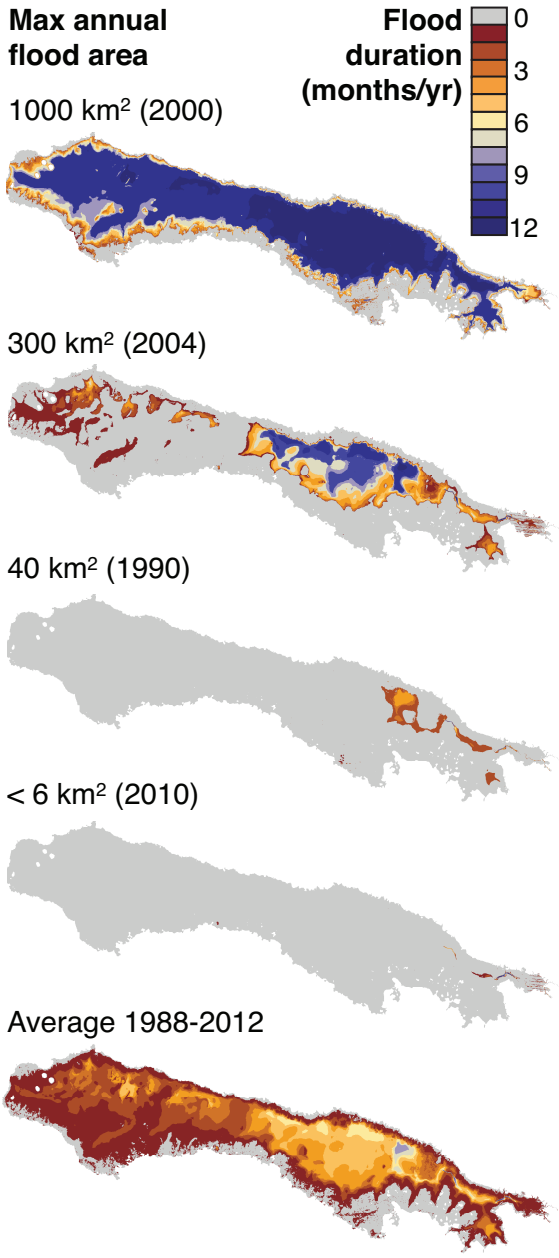

Figure 6: Maps of the Fortescue Marsh floodplain including flood duration isohyets over the rain year (Nov–Oct) representing examples of the main connectivity thresholds: wettest year observed in 2000 (F_{Amax} ~ 1000 km^2); a very large flood year in 2004 (F_{Amax} ~ 300 km^2); the long-term mean flood year in 1990 (F_{Amax} ~ 40 km^2) and a dry year in 2010 (F_{Amax} < 6 km^2) and the 1988–2012 average.

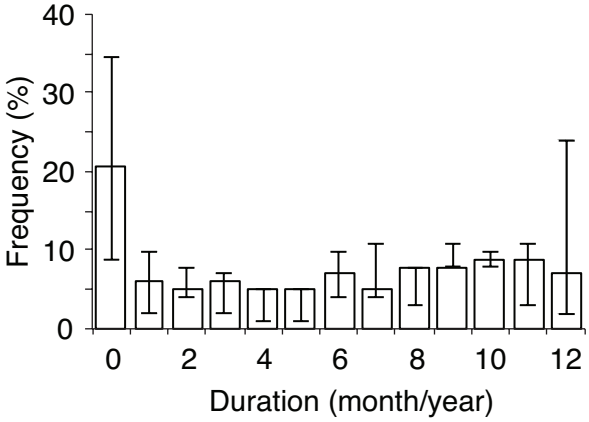

Figure 7: Frequency distribution of drought duration per annum (i.e. consecutive month with $F_A < 0$ km^2), with error bars representing the variation in the distribution when threshold for drought duration is defined as $F_A < \pm 56$ km^2 for the last century ($n = 100$ yr).

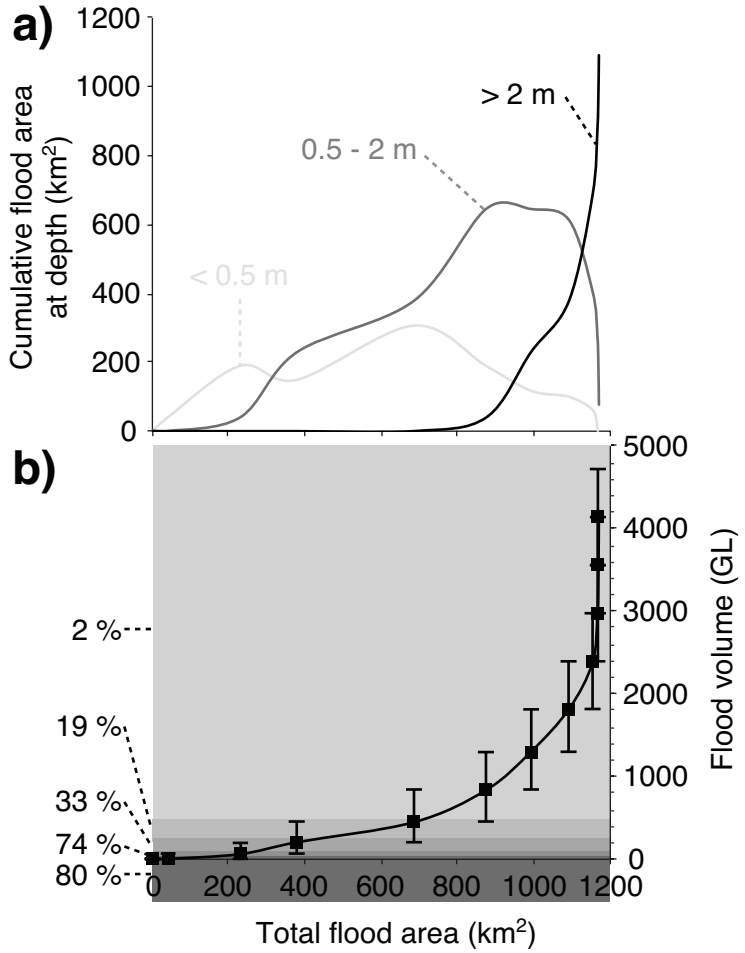

Figure 8: Total flood area at the Fortescue Marsh and **a)** its proportion occupied by water depth shallower than 0.5 m (light grey), between 0.5 and 2 m (dark grey) and deeper than 2 m (black) and **b)** the volume of surface water (black line) with century frequencies (% yr) at which different thresholds (grey shading) were attained.

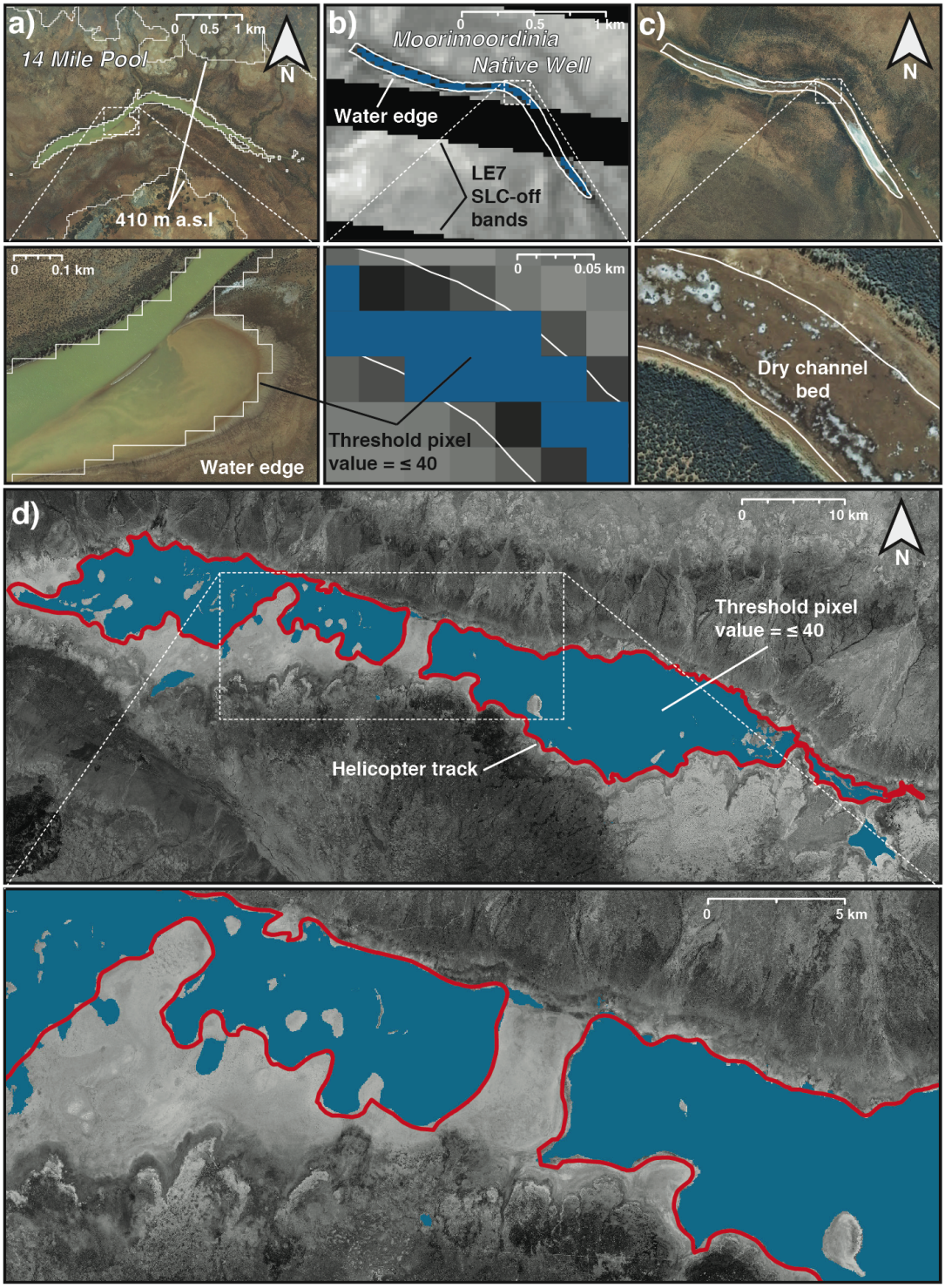
a)
0 0.5 1 km
14 Mile Pool
N
410 m a.s.l
b)
0 0.5 1 km
Moorimoordinia
Native Well
Water edge
LE7
SLC-off
bands
c)
N
0 0.1 km
Water edge
0 0.05 km
Threshold pixel
value = ≤ 40
Dry channel
bed
d)
0 10 km
N
Threshold pixel
value = ≤ 40
Helicopter track
0 5 km

1

2

Figure A1: Validation and groundtruthing of standing water on the Fortescue Marsh, including: **a)** standing water on the 14 Mile Pool extracted from Level 1T Landsat image (Jul 2010; solid white line = threshold pixel value ≤ 40; LT5; USGS) and close up against a 40-cm resolution ortho-photo (Jul 2010); delineation by GPS route tracking while walking along the water edge (1–2 m distance from standing water; solid white line) and close up against **b)** a Level 1T Landsat image of Moorimoordinia Native Well (Nov 2012; blue fill = threshold pixel value ≤ 40; LE7-SLC-off, USGS) and **c)** a RGB image showing the extent of the dry channel bed (Dec 2006; SPOT-5); **d)** delineation of standing water by GPS route tracking during a low altitude helicopter survey along the water plume of the Fortescue Marsh (2012 Feb 12; solid red line) and close up against standing water extracted from Level 1T Landsat image (2012 Feb 14; blue fill = threshold pixel value ≤ 40; corrected LE7-SLC-off; USGS), overlain on a 2.5 m resolution RGB image taken during dry season (Dec 2006; SPOT-5).

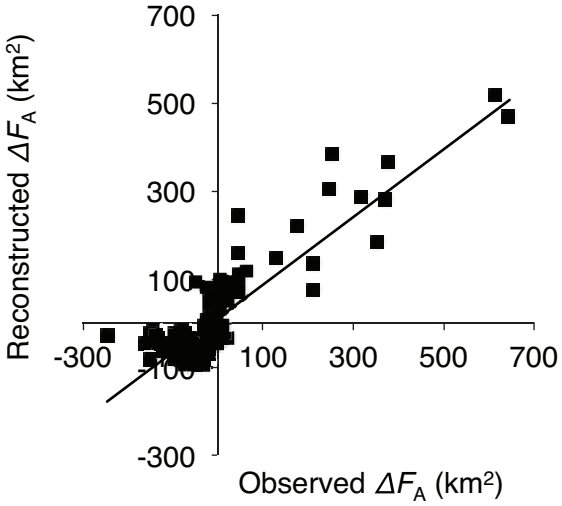

Figure A2: Observed against reconstructed monthly ΔF_A values ($n = 160$) for the 1988–2012 calibration period ($R^2_{adj} = 0.79$; $p\text{-}value < 0.001$).

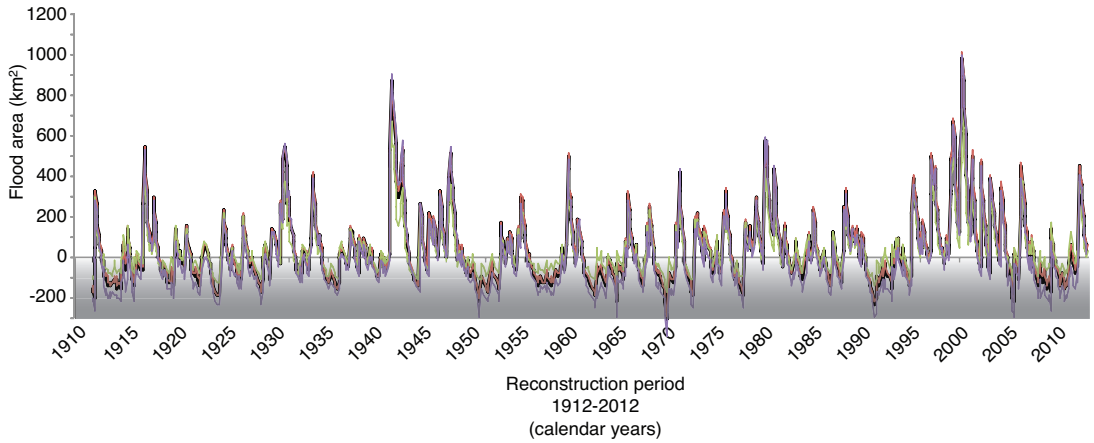

Figure A3: Surface water extent (F_A) at the Fortescue Marsh reconstructed using the final model based on the full 1988–2012 calibration period (black line) and the subsets for the 1998–2012 (red line) 1988–1997; 2005–2012 (green line), 1988–2004 (purple line) periods; $F_A \leq 0$ km^2 = no surface water evident on the Marsh (shaded).

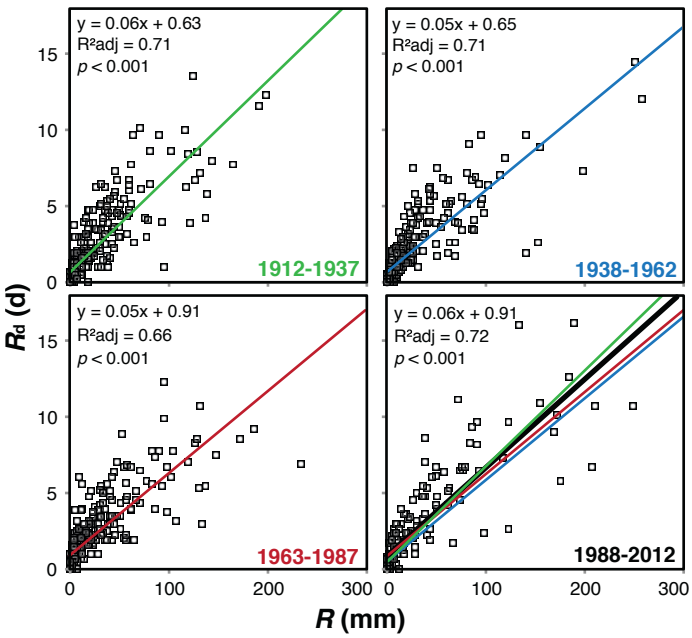

Figure A4: Collinearity between R and R_d over the last century (1912–1937; 1938–1962; 1963–1987) compared to the calibration months (1988–2012).